Progress in the development of ELM pace-making with non-axisymmetric magnetic perturbations in NSTX

2010 Nucl. Fusion 50 064016

(http://iopscience.iop.org/0029-5515/50/6/064016)

IOP Publishing and International Atomic Energy Agency Nuclear Fusion
Nucl. Fusion **50** (2010) 064016 (7pp) doi:10.1088/0029-5515/50/6/064016

Progress in the development of ELM pace-making with non-axisymmetric magnetic perturbations in NSTX

J.M. Canik[1], A.C. Sontag[1], R. Maingi[1], R. Bell[2], D.A. Gates[2], S.P. Gerhardt[2], H.W. Kugel[2], B.P. LeBlanc[2], J. Menard[2], S. Paul[2], S. Sabbagh[3] and V.A. Soukhanovskii[4]

[1] Oak Ridge National Laboratory, Oak Ridge, TN 37831, USA
[2] Princeton Plasma Physics Laboratory, Princeton University, Princeton, NJ 08543, USA
[3] Columbia University, New York, NY 10027, USA
[4] Lawrence Livermore National Laboratory, Livermore, CA 94551, USA

E-mail: canikjm@ornl.gov

Received 16 October 2009, accepted for publication 13 January 2010
Published 28 May 2010
Online at stacks.iop.org/NF/50/064016

Abstract
The application of non-axisymmetric magnetic perturbations has been shown to destabilize edge-localized modes (ELMs) in the National Spherical Torus Experiment. This ELM-triggering effect is used to controllably introduce ELMs into lithium-enhanced ELM-free H-mode discharges, reducing the typical impurity accumulation while maintaining high energy confinement. Recent improvements to the triggering techniques are described. The perturbation waveform has been improved, with large amplitude, short duration perturbations allowing rapid, highly reliable triggering, with reduced braking of toroidal rotation. The rapid triggering allowed the ELM frequency to be increased to over 60 Hz, leading to a reduction in the average ELM size. Combined with improved gas fuelling, this method has resulted in periods of stationary global conditions, although plasma profiles do continue to evolve.

PACS numbers: 52.55.Fa

(Some figures in this article are in colour only in the electronic version)

1. Introduction

A large amount of effort in the magnetic confinement fusion community is being expended on the control of edge-localized modes (ELMs). These instabilities are thought to be caused by coupled peeling and ballooning modes [1] driven by the steep pressure gradients and associated bootstrap currents typical of the edge of tokamak H-mode plasmas. The periodic ejections of particles and energy caused by ELMs pose a serious threat to the lifetime of plasma facing components (PFCs), and so the size of ELMs must be tightly controlled in ITER [2] and other future large tokamaks. Possible means of ELM control are reviewed in [3]; active control methods include suppression or mitigation using resonant magnetic perturbations (RMPs) as demonstrated in the DIII-D and JET tokamaks [4–7], and intentional triggering of ELMs at controllable frequency using pellet injection (e.g. as demonstrated in ASDEX-Upgrade [8]) or vertical plasma position jogs (studied in the TCV tokamak [9], and recently observed in NSTX [10]). Here we report on the development of a recently proposed ELM pacing technique, in which non-axisymmetric magnetic fields are used to trigger ELMs [11, 12].

While ELMs pose a threat to PFC lifetime, they also help to improve discharge performance by expelling particles and impurities, allowing for quasi-stationary conditions. Without ELMs, unless another transport mechanism is found to increase the particle transport (for example, the EDA mode observed in the Alcator C-mod tokamak [13], and the QH [14], and RMP [5] H-modes seen at DIII-D) the ELM-free H-mode typically shows a secular increase in density and impurity accumulation, which make this a necessarily transient operating scenario. An example of the non-stationary nature of ELM-free H-modes can be found in recent experiments in the National Spherical Torus Experiment (NSTX) studying the effects of lithium PFC coatings. In these discharges, lithium conditioning leads to the suppression of ELMs [15, 16], improved energy confinement and strong impurity accumulation [17] leading to radiated power that increases throughout the discharge. Carbon is the dominant low-Z impurity in these plasmas, with little core lithium contamination; the radiated power increase is

attributed to the accumulation of metallic species [17]. A method for controlling the density and impurity evolution in these lithium-enhanced H-modes has been demonstrated, in which ELMs are controllably restored by triggering them with non-axisymmetric magnetic perturbations [11]. Initial experiments showed the potential of this concept, with the induced ELMs leading to a reduction in the radiated power and line-averaged electron density while maintaining the high energy confinement caused by lithium conditioning (the energy confinement time can be as much as 20–50% higher with lithium coatings compared with bare carbon PFCs) [12]. Several areas for improving this technique were noted, including the need for reducing the size of the triggered ELMs, improving the reliability of the triggering and fully arresting the evolution of the density and radiated power.

The experimental details and physics of the destabilization of ELMs by non-axisymmetric magnetic perturbations are discussed elsewhere [12]; here we present the recent technical progress in the use of this triggering to perform ELM pace-making during the NSTX lithium-enhanced ELM-free H-modes. In section 2 the basic setup of the experiments is discussed. Section 3 presents the improvements made to the waveform of the perturbation used to trigger ELMs and in section 4 the optimization of the used triggered ELMs to improve discharge control is presented. Section 5 contains a discussion of these results and possible future directions.

2. Setup of experiments

NSTX is a mid-sized spherical torus, with major and minor radii of 0.85 and 0.65 m, respectively. The plasmas studied in the experiments presented here were highly shaped, with elongation of $\kappa = 2.4$–2.6, triangularity $\delta = 0.7$–0.8, and were near-double-null biased slightly to the lower X-point (dr^{sep}—the distance between the primary and secondary separatrices at the outboard midplane—was ∼5 mm). These experiments were performed with the ion grad-B drift direction favourable for H-mode access. The toroidal magnetic field was $B_t = 0.45$ T, and all discharges were heated with 4 MW of neutral beam injection. The plasma current was varied from 800 kA to 1 MA.

The non-axisymmetric magnetic perturbations are applied using a toroidal array of six coils located at the midplane, external but close fitting to the vacuum vessel. These coils are typically used for error field correction and resistive wall mode control [18], and can also be used to produce resonant perturbations for stochastic magnetic field experiments [19]. In the experiments presented here, these 'RWM coils' were configured to produce a field with a dominant toroidal mode number $n = 3$. The poloidal spectrum of the perturbations is quite broad [12], such that both the resonant and non-resonant components are strong; these cannot be separated in the NSTX experiments.

3. Improvements to ELM triggering

The initial experiments to prove the concept of using 3D field pulses to trigger ELMs *at will* showed a need to reduce the size of the triggered ELMs, since the average $\Delta W/W_{tot}$ was quite large at ∼10% (here ΔW is the energy ejected by an ELM and W_{tot} is the total plasma stored energy before the ELM). The large average ELM size was partially due to very large ELMs that were observed to be triggered following an $n = 3$ triggering pulse that failed to cause an ELM [12]. In order to avoid these large events and reduce the average ELM size, it is desirable to improve the triggering reliability. In addition, improving the triggering efficiency should allow the triggered ELM frequency to be increased, further decreasing the average ELM size. In the first set of experiments to improve the pacing of ELMs, the waveform of the triggering pulses was optimized in order to achieve these improvements in the triggering reliability and frequency, with the goal of reducing the size of the triggered ELMs.

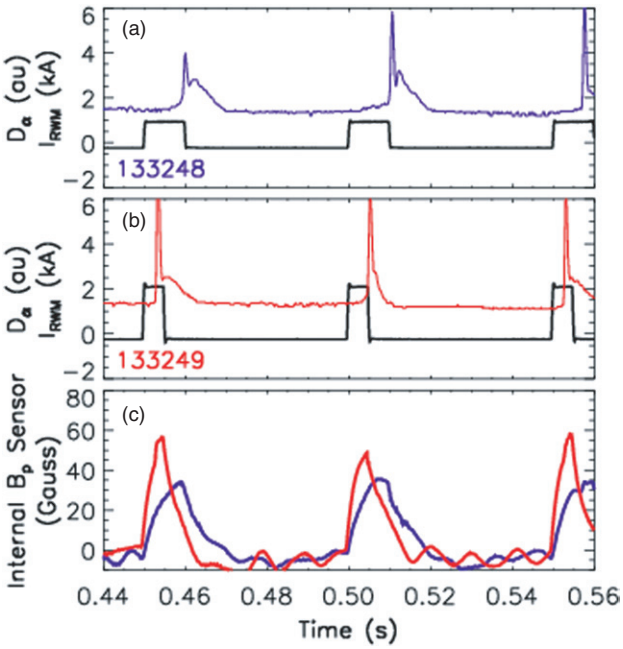

Figure 1. Faster ELM triggering with large perturbations: RWM coil current and D_α emission at (*a*) 1.0 kA and (*b*) 2.2 kA and (*c*) magnetic field measured inside the vessel.

Previous experiments showed a threshold perturbation strength needed in order to destabilize ELMs [12]. It was also observed that during ELM pacing in lithium-enhanced discharges, ELMs were triggered typically 10 ms after the $n = 3$ field application; this delay may have been set by the penetration time of the fields through the vessel, estimated as ∼4 ms. To test this, the amplitude of the $n = 3$ field was considerably increased, so that the threshold field inside the vessel could be reached more quickly. Figure 1 shows time traces of the RWM coil current waveform, along with the D_α in the upper divertor. At a current of ∼1.0 kA in the RWM coils (upper frame), the ELMs are triggered roughly 8 ms after the start of the $n = 3$ pulse. This is consistent with previous results at these current levels. The perturbed field inside the vessel is measured by magnetic sensors located on passive stabilization plates above and below the midplane, ∼10 cm from the plasma; these are typically used for RWM detection [18]. The field measured by an internal sensor is shown in the third frame of figure 1, and confirms that the field takes several milliseconds to penetrate into the plasma. To reach the destabilization threshold and trigger the ELMs more quickly, the amplitude

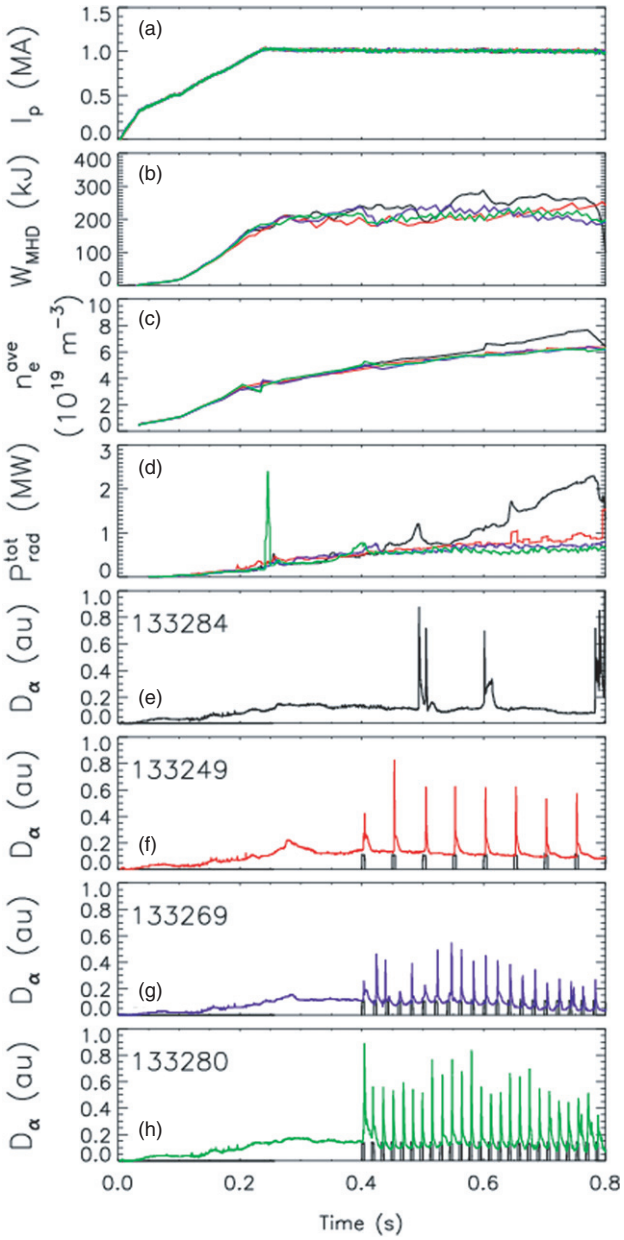

Figure 2. ELM triggering at $I_p = 1.0$ MA with RWM coil current pulses of 2.2 kA at frequencies of 20, 50 and 62.5 Hz: (*a*) plasma current, (*b*) stored energy, (*c*) line-averaged density, (*d*) radiated power and (*e*)–(*h*) D_α and $n = 3$ pulse timing.

of the perturbation was increased: when the RWM coil current was increased to 2.2 kA, the time it took to trigger an ELM was cut roughly in half (figure 1). In this case, the ELM is triggered in ∼4 ms, which is comparable to the field penetration time based on the internal measurements. Since the current limit in the RWM coil is ∼3 kA, the penetration time remains the limit to the triggering speed; ELMs could presumably be triggered even faster with internal coils.

By achieving more rapid ELM triggering, the likelihood of a pulse triggering an ELM is also increased (for fixed pulse duration), thereby improving the triggering reliability. Using the large amplitude $n = 3$ pulses, the reliability of the ELM triggering has been increased up to 100% (figure 2; previously ∼75% triggering efficiency had been achieved

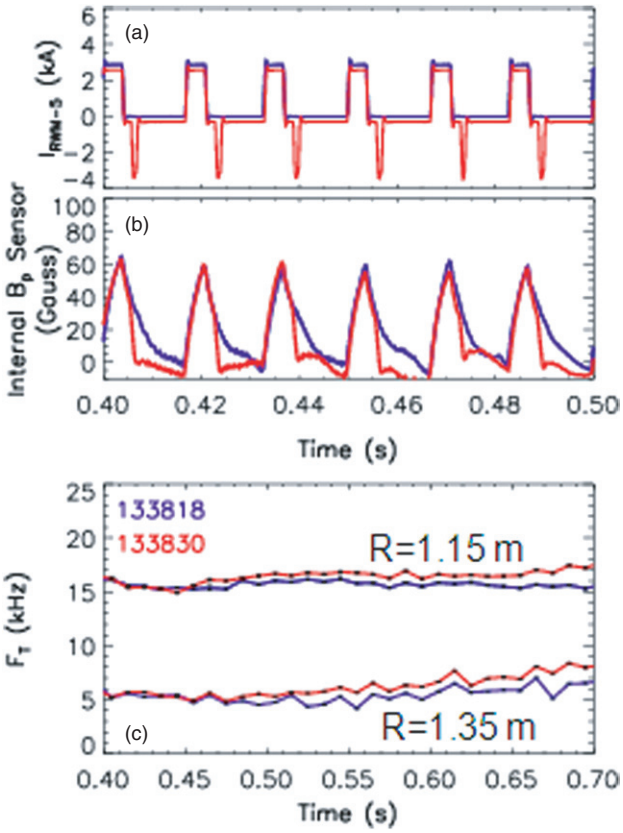

Figure 3. Optimized pulse shape (red): (*a*) current in perturbation coils, (*b*) internal magnetic measurement and (*c*) toroidal rotation at $R = 1.15$ and 1.35 m (15 cm outboard of the axis and 10 cm inboard of the separatrix, respectively).

[12]). Furthermore, the rapid triggering has allowed the ELM frequency to be significantly increased, while still maintaining 100% triggering efficiency. This is illustrated in figure 2 for triggering frequencies of 20, 50 and 62.5 Hz. These plasmas have the shape parameters listed in section 2, with a plasma current of 1 MA. In all cases, an ELM is triggered on every pulse, so that the ELM frequency matches the pulse frequency, demonstrating the reproducibility of this technique. The ELM pace-making was successful at every frequency of arresting the total radiated power and reducing the line-averaged electron density n_e compared with the reference discharge (black curves) which is a nearly ELM-free lithium-enhanced H-mode plasma.

Although the ELM pacing by this method is successful at improving the density and impurity evolution of the discharge, the continual application of these large perturbations leads to a reduction in confinement (figure 2(*b*)), and also to large time-average magnetic braking of the toroidal rotation. To reduce the magnetic braking, the waveform of individual field pulses was improved by adding a short pulse of the opposite sign to each $n = 3$ pulse. The intention was to counteract the vessel eddy currents, so that the field internal to the vessel could be reduced more rapidly. The results of this addition are shown in figure 3, where the magnetic field measured by a sensor internal to the vessel is shown. In the case with the fast $n = 3$ field reversal, the internal magnetic field decays back to near zero significantly faster than in the case with

single-sign pulses. As a result, the time-average perturbed field in the plasma is reduced, which leads to a reduction in the (again time-averaged) magnetic braking. This is apparent when comparing the toroidal rotation using the two waveforms: with the addition of the negative-going spikes, the rotation is increased compared with the case without (figure 3). In the absence of internal perturbation coils that would allow the field to be manipulated much faster, this technique may be necessary to ensure that the adverse impact on the plasma performance due to the $n = 3$ fields is minimized. With internal coils, the vessel penetration time would be removed as a limiting factor, and the counteraction of eddy currents would be unnecessary. The increase in achievable ELM frequency and reduction in time-averaged braking enabled by such coils would depend on the time scales of the triggering physics processes involved, which are not well known (e.g. the penetration time of resonant fields [20] may be a controlling factor).

4. Optimization of ELM pacing of Li-enhanced ELM-free H-modes

A primary goal of increasing the triggered ELM frequency is to reduce the energy expelled by each individual ELM. As noted from previous experiments [12], the ELMs that are triggered during what would otherwise be ELM-free H-modes are typically quite large, with values of $\Delta W/W_{\rm tot}$ of 10–20% (the pedestal stored energy is typically ~30% of the total for NSTX, so that the largest ELMs expel as much of half of the pedestal energy). For natural ELMs, higher frequencies yield smaller energy ejection [21]; this observation has led to attempts to reduce ELMs through pace-making, i.e. externally increasing the frequency above its natural value. While this dependence is not guaranteed to hold for the triggered ELMs, it is hoped that similar reductions can be achieved in the ELM size by increasing the triggering frequency.

The improvements to the perturbation waveform and triggering efficiency have enabled triggering of higher frequency ELMs. Previously frequencies up to ~30 Hz had been achieved [12], compared with over 60 Hz triggered as displayed in figure 2. Figure 4 shows the variation of the ELM size with triggering frequency for the 1 MA plasmas described in section 2; in all cases shown, the RWM coil current waveform *without* negative-going spikes (cf figure 3) is used. While a reduction in average ELM size is evident as the frequency is increased, even at the highest frequency achieved the average value of $\Delta W/W_{\rm tot}$ remains quite large at ~10%. This is far above the fractional ELM size that is acceptable in future large tokamaks (for reference, to mitigate damage to plasma facing materials, the ELM size in ITER must be restricted to 0.3% of the total stored energy [2]), and clearly further improvements are necessary to show the extrapolability of this triggering method. Fortunately, the reduction in ELM size with frequency was more pronounced in plasmas with similar shapes but lower plasma current at $I_{\rm p} = 800$ kA. In this case, the average ELM size was reduced to 5% of the total stored energy at 60 Hz triggering, compared with 10% at similar frequencies of 1 MA plasma current (figure 4). Since the frequency of the $n = 3$ pulses remains limited by the penetration through the vessel, it is likely that significantly higher frequencies could be achieved with perturbation coils

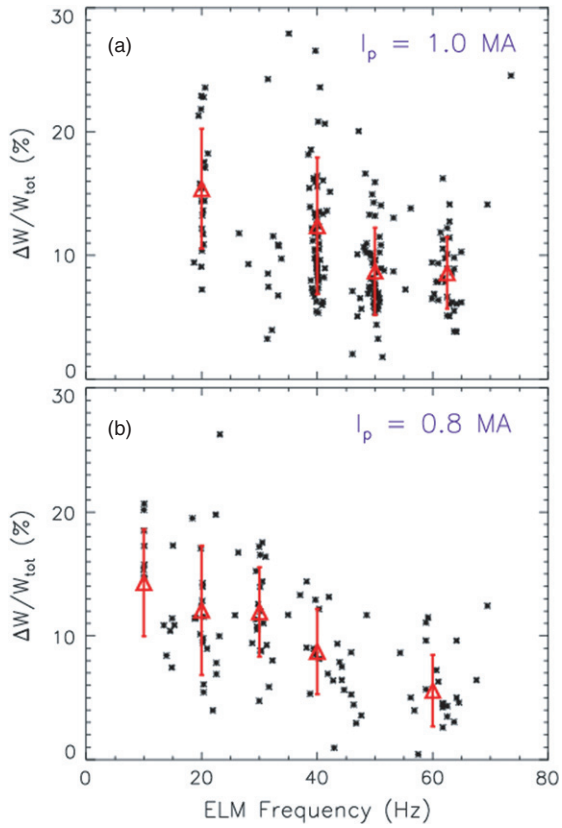

Figure 4. ELM size dependence on frequency for plasma currents of (*a*) 1.0 and (*b*) 0.8 MA, Points represent individual ELMs; triangles are the average value binned around the triggering frequencies, and error bars are the standard deviation of the data set.

located internal to the vacuum vessel. This should then allow a further reduction in the ELM size. However, it should be noted that even at the highest frequencies achieved, infrequent large ($>10\%\Delta W/W_{\rm tot}$) ELMs remain. Although further analysis is required to quantify the effect, it is possible that the reduced ELM size at $I_{\rm p} = 800$ kA is due to the expected smaller ELM-affected area at high values of q_{95} [22]. Furthermore, the current dependence suggests that the reduction in ELM size previously observed at high plasma elongation [12] may have been in fact due to the change in edge safety factor during the shaping scan.

Although we have shown that high-frequency ELM triggering can be achieved, this is not ideal for maintaining high-performance discharges. To find the optimal operating point, a scan of the triggering frequency was performed while holding other discharge parameters constant (shape parameters are as described in section 2, and the plasma current reduced to $I_{\rm p} = 800$ kA). Time traces of several frequencies during this scan are shown in figure 5. As the D_α traces show, in this set of discharges somewhat less than 100% triggering was achieved at the higher pulse frequencies (typically ~80% triggering was achieved for the first ~300 ms of pacing, decreasing to ~50% later in the discharge). However, in all cases the radiated power is significantly reduced near the end of the discharge compared with the control, ELM-free case, and the line-average density reduced. The stored energy is relatively unaffected by the restoration of ELMs; as discussed below, confinement is reduced in the highest frequency case by a rotating MHD

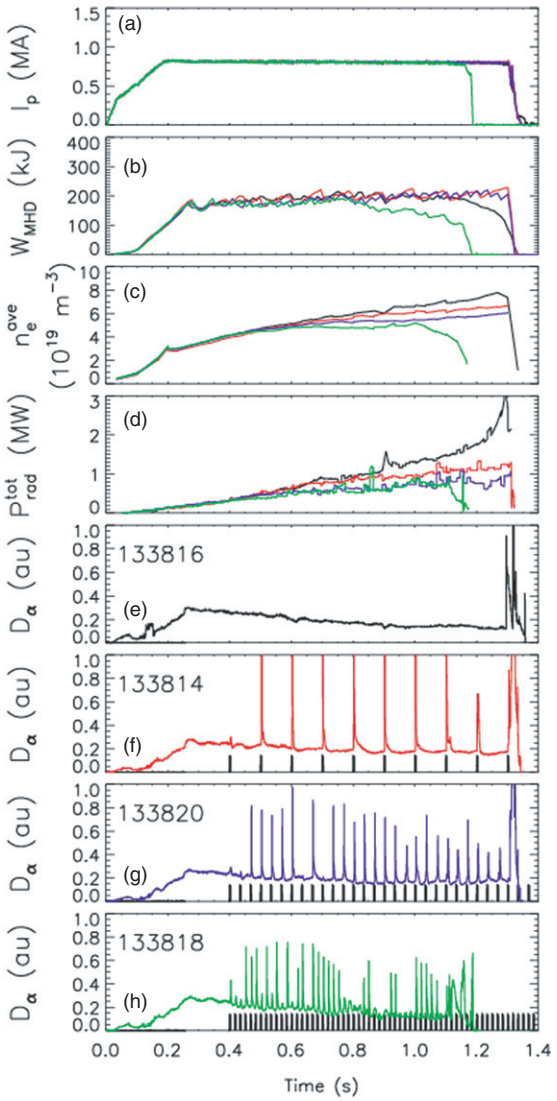

Figure 5. ELM triggering at $I_p = 800$ kA with RWM coil current pulses of 2.7 kA at frequencies of 10, 30 and 60 Hz: (*a*) plasma current, (*b*) stored energy, (*c*) line-averaged density, (*d*) radiated power and (*e*)–(*h*) D_α and $n = 3$ pulse timing.

mode beginning at $t \sim 0.8$ s (which also apparently affects the triggering reliability).

The total radiated power from several times during these discharges is shown in figure 6: at $t = 0.4$ s, when the $n = 3$ triggering begins, at $t = 0.75$ s, and at $t = 1.25$ s, near the end of the discharge. These are shown for the full range of pulse frequencies tested. With no ELM triggering (frequency of 0 Hz), the radiated power increases throughout the discharge, with a strong increase near the end of the discharge leading to more than half the input power lost through radiation (this leads to a reduction in the plasma stored energy, as shown in figure 5). As the frequency is increased, the radiated power is quickly arrested, being held to a value of less than 1 MW ($\leqslant$25% of the input power) throughout the discharge for triggering frequencies of 20 Hz and above. Although the radiation does increase modestly with time during these lower-frequency cases, the magnitude of the radiation does not affect the stored energy. The impact of the pulse frequency on

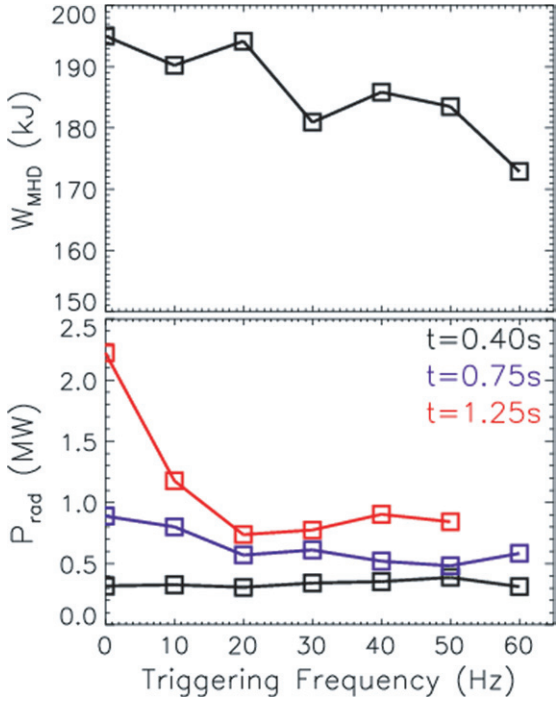

Figure 6. Dependence of the (*a*) time-averaged stored energy and (*b*) total radiated power on $n = 3$ pulse frequency.

plasma stored energy is also shown; this is averaged from $t = 0.5$ to 0.75, which is during the triggering phase but before the MHD activity that occurs at higher triggering frequency. The time-averaged stored energy shows a decrease as the frequency is increased, although this reduction is modest; the average stored energy is ~10% lower with 60 Hz triggering compared with the ELM-free discharge. This confirms that the restoration of ELMs to the lithium-enhanced plasmas is compatible with largely retaining good confinement enabled by lithium conditioning. Furthermore, for the purpose of controlling NSTX discharge evolution, this indicates that lower frequency triggering may be preferable from the standpoint of reducing the impurity accumulation while minimizing the impact on confinement, although in any case a high frequency is likely to be necessary to limit the ELM size.

To more fully control the density evolution, the ELM pace-making was combined with more controlled particle fuelling. Typically, NSTX discharges are fuelled using a gas valve located on the centre post, which eases H-mode access [23]. Due to limited space, this puff system has a slow time response, such that strong fuelling persists throughout the discharge. In order to reduce the gas following plasma startup, the gas puff using this centre stack valve was gradually reduced and replaced with fuelling from a supersonic gas injector [24]. This allowed the amount of gas puffed into the plasma in later stages of the discharge to be reduced by ~30%. This improved fuelling was then combined with ELM pace-making with the $n = 3$ fields to optimize density control. The method was successful in achieving stationary line-averaged density and total radiated power evolution for ~300 ms, as shown in figure 7. This quasi-stationary period is typically terminated by rotating MHD activity, as shown in the MHD sensor data shown. This mode has a toroidal mode number of $n = 1$

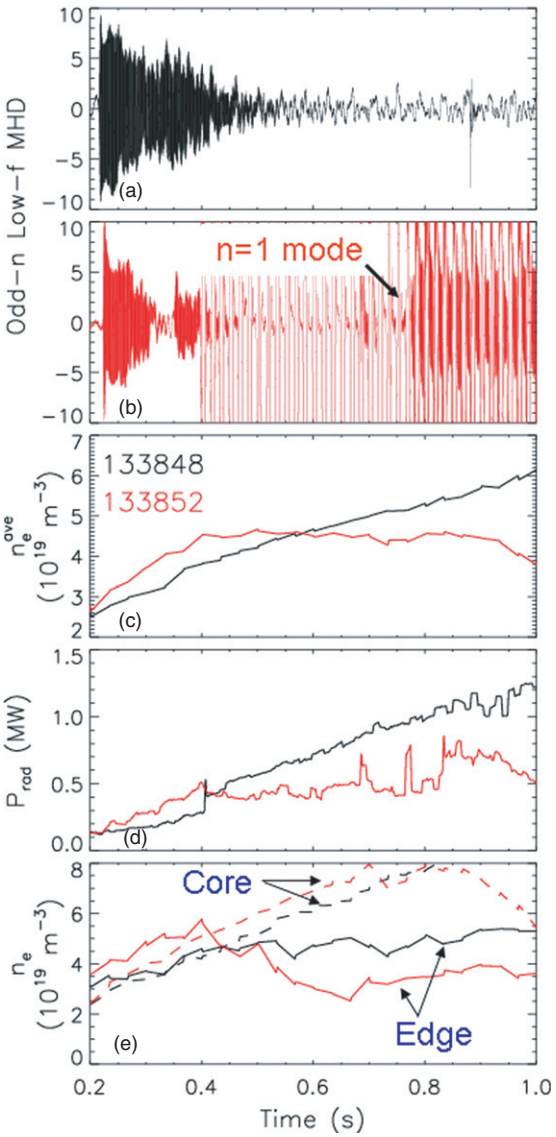

Figure 7. Combined improved fuelling and ELM pacing: (*a*) and (*b*) odd-*n* MHD activity, (*c*)line averaged electron density, (*d*) total radiated power and (*e*) local electron density at the axis (dashed lines) and the edge (solid lines; 8 cm inside the separatrix).

based on fitting of toroidal array of magnetic sensors and a frequency that matches the toroidal rotation frequency at the $q = 2$ surface, suggesting that this is a 2/1 neoclassical tearing mode; the behaviour of these modes in NSTX has been reported elsewhere [25]. When this mode arises, the performance of the discharge is significantly degraded, with the stored energy decreasing by 20–30% (see, e.g. the high-frequency triggering case shown in figure 5).

Although these global parameters are successfully arrested, the density profile continues to evolve throughout the ELM-triggering phase. As shown in figure 7(*e*), the local electron density on the magnetic axis (dashed lines) increases monotonically in the ELM-paced discharge, with a similar rate of increase to the reference ELM-free discharge. The edge density, on the other hand, shows a strong decrease in time following the application of the $n = 3$ pulses (the timing of the pulses can be seen from the pick-up of the perturbation on the odd-*n* MHD sensor shown in panel (*b*)). The constancy of the line-averaged density is therefore due to a decrease in the edge density, combined with an increasing core density that appears not to be strongly affected by the presence of ELMs. Similar behaviour is observed in the local carbon and radiated power densities: the values on axis increase relatively unchanged by the presence of ELMs, while the edge values decrease in time after the ELM pacing begins. While the ELM pacing is clearly effective at controlling the edge plasma, more development is required to bring the discharge to true stationary conditions.

5. Discussion and conclusions

Recent experiments have led to significant improvements in the method of using non-axisymmetric magnetic perturbations to perform ELM pace-making during lithium-enhanced ELM-free H-modes in NSTX. Achievements include improved triggering reliability by maximizing the strength and reducing the duration of the perturbation pulses. This has allowed 100% ELM triggering to be maintained at frequencies over 60 Hz. Further improvements to the triggering waveform have allowed a reduction in magnetic braking by applying short negative-going pulses to each triggering pulse, decreasing the time-averaged perturbed field inside the vessel.

The size of the triggered ELMs, while typically large with $\Delta W/W_{tot} \sim 10\%$, can be decreased by increasing the triggering frequency. This has allowed the ELM size to be reduced to ∼5% at a plasma current of 800 kA, while ELM sizes remain at ∼10% at a higher current of 1 MA. High-frequency triggering does not appear to be necessary for discharge control at $I_p = 800$ kA, with the total radiated power being largely arrested for pulse frequencies above 20 Hz; on the other hand, the stored energy shows a decrease as the frequency is increased, so that the optimal triggered ELM frequency for NSTX is 20–30 Hz. The impact of the ELMs on confinement is fairly small, in any case, with the stored energy being decreasing by only ∼10% at the highest triggering frequency.

The controlled restoration of ELMs to lithium conditioned discharges, combined with improved particle fuelling, has resulted in a period of stationarity in the global discharge parameters lasting ∼300 ms. However, plasma profiles continue to evolve during this period, with the core electron, carbon and radiated power densities increasing at a rate similar to the control discharge. The edge values of the parameters decrease in time, giving rise to the global stationary conditions. Further development is therefore necessary to reduce the core particle confinement; this may be achieved, for example, with electron cyclotron heating of the core electrons, such as has been used at ASDEX-Upgrade to reduce metallic impurity accumulation [26].

These recent accomplishments show the potential for the combination of lithium coatings and ELM pacing using 3D fields to provide a stationary, high-performance plasma. The modest impact of the triggered ELMs on the energy confinement suggests that the improved confinement caused by lithium coatings can be retained when combined with ELM pacing. The size of the triggered ELMs is rather large even in the best case, but a clear path to reducing the ELM size through high-frequency triggering with internal coils has been identified. This may be an attractive operating scenario for

a device such as an ST-based component test facility [27], where the requirements on the maximum ELM size may be less stringent [28]. However, the technique clearly requires more development in order to control the core particle confinement in addition to the edge.

Acknowledgments

This research was sponsored in part by the US Department of Energy Contracts DE-AC05-00OR22725, DE-AC02-09CH11466 and DE-FG02-99ER54524.

References

[1] Snyder P.B. *et al* 2004 *Plasma Phys. Control. Fusion* **46** A131
[2] Federici G. *et al* 2003 *J. Nucl. Mater.* **313–316** 11
[3] Oyama N. 2008 *J. Phys. Conf. Ser.* **123** 012002
[4] Evans T.E. *et al* 2004 *Phys. Rev. Lett.* **92** 235003
[5] Evans T.E. *et al* 2008 *Nucl. Fusion.* **48** 024002
[6] Liang Y. *et al* 2007 *Phys. Rev. Lett.* **98** 265004
[7] Alfier A. *et al* 2008 *Nucl. Fusion* **48** 115006
[8] Lang P.T. *et al* 2004 *Nucl. Fusion* **44** 665
[9] Degeling A.W. *et al* 2003 *Plasma Phys. Control. Fusion* **45** 1637
[10] Gerhardt S.P. *et al* 2010 *Nucl. Fusion* **50** 064015
[11] Canik J.M. *et al* 2010 *Phys. Rev. Lett.* **104** 045001
[12] Canik J.M. *et al* 2010 *Nucl. Fusion* **50** 034012
[13] Greenwald M. *et al* 2000 *Plasma Phys. Control. Fusion* **42** A263
[14] Burrell K.H. *et al* 2001 *Phys. Plamas* **8** 2153
[15] Mansfield D. *et al* 2009 *J. Nucl. Mater.* **390–391** 764
[16] Maingi R. *et al* 2009 *Phys. Rev. Lett.* **103** 075001
[17] Paul S. *et al* 2009 *J. Nucl. Mater.* **390–391** 211
[18] Sontag A.C. *et al* 2005 *Phys. Plasmas* **12** 056112
[19] Yan L. *et al* 2006 *Nucl. Fusion* **46** 858
[20] Becoulet M. *et al* 2009 *Nucl. Fusion* **49** 085011
[21] Maingi R. *et al* 2005 *J. Nucl Mater.* **337–339** 727
[22] Becoulet M. *et al* 2005 *J. Nucl. Mater.* **337–339** 677
[23] Maingi R. *et al* 2004 *Plasma Phys. Control. Fusion* **46** A305
[24] Soukhanovskii V.A. *et al* 2004 *Rev. Sci. Instrum.* **75** 4320
[25] Gerhardt S.P.*et al* 2009 *Nucl. Fusion* **49** 032003
[26] Gruber O. *et al* 2009 *Nucl. Fusion* **49** 115014
[27] Peng Y.-K.M. *et al* 2005 *Plasma Phys. Control. Fusion* **47** B263
[28] Peng Y.-K.M. *et al* 2008 *Proc. 22nd Int. Conf. on Fusion Energy 2008 (Geneva, Switzerland, 2008)* (Vienna: IAEA) CD-ROM file FT/P3-14 and http://www-naweb.iaea.org/napc/physics/FEC/FEC2008/html/index.htm